Supporting Information: Polyolefins formed by chain walking catalysis - a matter of branching density only?

Ron Dockhorn,[†,‖] Laura Plüschke,[†,‡,‖] Martin Geisler,[†,‡] Johanna Zessin,[†,‡] Peter Lindner,[¶] Robert Mundil,[§] Jan Merna,[§] Jens-Uwe Sommer,[*,†,‡] and Albena Lederer[*,†,‡]

Leibniz Institute of Polymer Research Dresden, Hohe Strasse 6, 01069 Dresden, Germany, Technische Universität Dresden, 01069 Dresden, Germany, Institute Laue-Langevin (ILL), 6 Rue Jules Horowitz, 38042 Grenoble, France, and University of Chemistry and Technology Prague, Technická 5, 16628 Prague 6, Czech Republic

E-mail: sommer@ipfdd.de; lederer@ipfdd.de

Contents

List of Figures

[*]To whom correspondence should be addressed
[†]Leibniz Institute of Polymer Research Dresden, Hohe Strasse 6, 01069 Dresden, Germany
[‡]Technische Universität Dresden, 01069 Dresden, Germany
[¶]Institute Laue-Langevin (ILL), 6 Rue Jules Horowitz, 38042 Grenoble, France
[§]University of Chemistry and Technology Prague, Technická 5, 16628 Prague 6, Czech Republic
[‖]Both authors contributed equally to this work

List of Tables

Experimental Results

Instrumentation

High temperature size exclusion chromatography (HT-SEC) was performed with a PL-GPC 220 (Agilent Technologies, US) with an online degasser, an online preinjection filter and two PLgel Olexis columns (Agilent Technologies, US) filled with polystyrene as a packing material (13 μm nominal particle size). Measurements took place at an operating temperature of 150 °C. 1,2,4-Trichlorobenzene was used as an eluent. The flow rate was set to 1 mL·min^{-1}. Samples were dissolved between 1-2 h depending on the respective topology. The injection volume was set to 200 μL. The chromatograph was coupled to four consecutive detectors namely a DAWN® HELEOS™-II light scattering photometer with 18 angels (MALLS, Wyatt Technology, US), a DYNAPRO® Nanostar™- (DLS, Wyatt Technology, US), a four capillary viscometer (VISCO, Agilent Technologies, US) and a differential refractometer (dRI, Agilent Technologies, US). The Visco and dRI detector are arranged parallely which requires a 50/50 split of the eluent flow. The DLS is connected to the MALLS detector using an optical fiber positioned at detector channel 12 (99° relative to the incident laser beam). For normalization of MALLS photodiodes, adjustment of interdetector delays and band broadening a 30kDa polystyrene standard (PSS, DE) with narrow molar mass distribution was used. For determination of the dRI constant a 200 kDa polystyrene standard (PSS, DE) was used. Ambient SEC was performed using HPLC pump (Knauer, DE) coupled to ETA-2020 dRI detector (WGE Dr. Bures, DE) and a DAWN® Eos™- MALLS detector with three channels (Wyatt Technology, US). A PL Mixed C column (Agilent Technologies, US) with a nominal particle size of 5 μm was used for separation. The flow rate was 1 mL·min^{-1} and the injection volume was 25 μL.Refractive index increments $\delta n/\delta c$ were determined assuming a total mass recovery $\delta n/\delta c_{THF,25°C}$=0.080 mL/g and $\delta n/\delta c_{TCB,150°C}$=-0.100 mL/g. The raw data was processed and analyzed using ASTRA 6 (Wyatt Technology, US). Zimm Model (fit degree 1) was applied for static light scattering calculations. All sample averages and standard deviations were calculated from 3 determinations implying 3 separate dissolutions à 3

injections with a concentrations between 3.5-4.0 mg/mL.

Nuclear magnetic resonance (NMR) spectra were partly recorded on a Avance 500 NMR spectrometer (Bruker-Biospin, DE) using $CDCl_3$ as a solvent. The ^1H analyses acquisition time was $1.59s$ and the relaxation delay 10 s. The ^{13}C NMR spectra (125.77 MHz) were recorded using 90° ^{13}C pulses and inverse gated ^1H decoupling. The acquisition time was 1.05 s and the relaxation delay 10 s. Residual ^{13}C-NMR spectra were collected on a Bruker Avance DRX 500 spectrometer using 90° pulse and a relaxation delay of $10s$. The chemical shifts were referenced internally to the major backbone methylene carbon resonance, which was taken at $\delta = 30ppm$ from tetramethylsilane. The total number of branching N_{Br} from ^1H NMR was calculated using Eq. (32) by integrating methyl proton signals with respect to signals of all protons in the spectrum. N_{Br} from ^{13}C NMR was obtained by summing up integrals of signals obtained in the methyl region ($\delta \geqslant 20.06ppm$). The interpretation of ^{13}C NMR spectra was based on the previously published literature.[1]

Small Angle Neutron Scattering (SANS) experiments were performed at the D11-instrument at the ILL in Grenoble, France. Measurements were performed at two wavelengths of 6 Å and 4.6 Å and two detector distances 8 m and 1.4 m resulting in momentum transfer range of $q = 0.04298\,\text{Å}^{-1} - 0.45\,\text{Å}^{-1}$ and $q = 0.00753\,\text{Å}^{-1} - 0.08617\,\text{Å}^{-1}$, respectively. The samples were dissolved in THF-d8 for 24 h and transferred into Hellma® precision cells. The sample volume was 1 mL. The scattering intensities were normalized with a standard water measurement. The solvent was separately measured, normalized and substracted from the solution data. Each sample was measured at five concentrations between $0.7 - 5\,\%$.

Atomic Force Microscopy (AFM): Samples were dissolved in TCB with $c = 10^{-2}$ mg/mL. The hot solution was transferred onto highly oriented pyrolytic graphite (HOPG) substrate and spin coated for 40 s with 2000 rpm and 100 rpm acceleration. The coated substrate was dried with nitrogen stream. The thin parallel lines visible in the AFM images originate prom the highly oriented pyrolytic graphite (HOPG) substrate and are regularly occurring edges on the substrate's surface. Due to spin-coating treatment, the deposited

CW structures entangle along these edges and expose the predicted bottle-brush shape.

Chemicals

THF for SEC measurements was purchased from Acros Organics (DE) and stabilized with 0.025 % Butylated Hydroxytoluene (BHT, Roth, $\geq$ 98 %) to prevent autooxidation. THF for SLS and DLS was purchased from Acros Organics (DE) with a purity of 99.5 % (stabilized, extra dry over molecular sieve). 1,2,4-Trichlorobenzene was purchased from Sigma Aldrich with a purity of $\geq$ 99 % and stabilized with 1 g/L BHT to prevent thermo-oxidative degradation. THF-d8 was purchased from Euriso-Top (France) with a residual water content of $\leq$ 0.05 %. All manipulations with air-sensitive compounds were done using Schlenk techniques. Chlorobenzene was dried over CaH_2 and freshly distilled before use. Ethylene (99.9 %, Linde) was purified by passing through the column packed with deoxygenating catalyst and molecular sieves.

Catalyst synthesis

Palladium-α-diimine complex [(N,N'-bis(2,6-diisopropyl)butane-2,3-diimine)

$Pd(CH_2)_3COOCH_3]$ + $[BAr^F_4]^-$ (Ar'=3,5-bis(trifluoromethyl)phenyl) was prepared according to the literature procedure[2,3] (see Figure SS1).

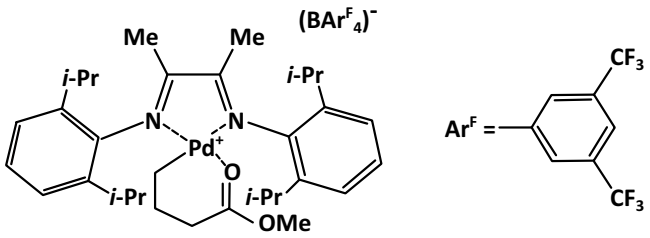

Figure S1: Palladium-α-diimine complex catalyst for synthesis of CWPE1-CWPE9, CW-PEx.

Polymerization procedure

A 100 ml Fisher-Porter tube with a magnetic stirring bar was charged with the appropriate amount of solid catalyst (c = 0.3 mg/mL for all analytes but CWPEx, c =

0.6 mg/mL). The desired volume of dry chlorobenzene was transferred via cannula to the reaction ampule. After stirring for 10 min at the desired temperature, the polymerization was started by the saturation of the reaction mixture with ethylene. Absolute ethylene pressure (8 bar, 7 bar on the gauge) was controlled by a gas regulator. For the polymerizations at 0.14 or 0.05 bar of ethylene, a mixture of ethylene and nitrogen was prepared and bubbled through the reaction mixture. After allotted polymerization time the ethylene pressure was released, and the reaction was quenched by the addition of 0.3 ml of triethylsilane. The chlorobenzene was evaporated on a rotary evaporator. Obtained polyethylene was dissolved in toluene and passed through a column packed with silica gel and alumina to remove the rest of the catalyst. Then, the solvent was evaporated and obtained polymer was dried under vacuum overnight at 50 °C.

Theoretical Background

The connection between molar mass and R_{g} is given by power law

$$R_{\mathrm{g}} = K \cdot M^{\nu} \tag{1}$$

in which the scaling between molar mass and size is topologically characteristic and is given by the exponent ν. While R_{g} is defined geometrically, the hydrodynamic radius R_{H} is also dependent on the solvation state of the polymer. It is expressed by

$$R_{\mathrm{H}} = \frac{k_B \cdot T}{6\pi\eta_0 D} \ , \tag{2}$$

where k_B is the Boltzmann´s constant, T is the absolute temperature, η_0 is the viscosity of the solvent, and D is the translational diffusion coefficient. The intrinsic viscosity is calculated from

$$[\eta] = \lim_{c \to 0} \left(\frac{\eta - \eta_0}{\eta_0} \frac{1}{c} \right) = \frac{10\pi}{3} N_A \frac{R^3}{M} \tag{3}$$

in which η is the viscosity of the dissolved macromolecules. The intrinsic viscosity $[\eta]$ is related to R_g and molar mass by the Flory-Fox[4,5] relationship with

$$[\eta] = \Phi \frac{R_g^3}{M} \tag{4}$$

with the Flory parameter Φ. $[\eta]$ can also be expressed by power law as Kuhn-Mark-Houwink-Sakurada equation

$$[\eta] = K_\eta \cdot M^\alpha \tag{5}$$

where the exponent α is related to the topology of the molecule. Using the intrinsic viscosity another hydrodynamic radius can be calculated via

$$R_\eta = \left(\frac{[\eta]\, M}{(10\pi/3)\, N_A} \right)^{1/3} \tag{6}$$

Alternatively, the branching density can be expressed using the contraction factor accounts for

$$g = \left(\frac{R^2_{g_{BRA}}}{R^2_{g_{LIN}}} \right)_M \tag{7}$$

which gives the size reduction of a branched polymer $R^2_{g_{BRA}}$ compared to its linear analogue $R^2_{g_{LIN}}$ at definite molar mass. While g is defined by R_g the contraction factor can also be calculated from $[\eta]$ with

$$g' = \left(\frac{[\eta]_{BRA}}{[\eta]_{LIN}} \right)_M \tag{8}$$

that can be more accurate especially for small macromolecules when SLS reaches its limitations regarding resolution. Both contraction factors are correlated by the branching index ε by

$$g' = g^\varepsilon \ . \tag{9}$$

Theoretical values are given with $\varepsilon = 0.5$ for linear chains and $\varepsilon = 1.5$ for highly branched structures. Long chain branching can be quantified by

$$LCB = 1000 \cdot B \cdot \frac{M_{\mathrm{RU}}}{M} \tag{10}$$

where $M_{\mathrm{RU}} = 28.05\, g/mol$ is the molar mass of the repeating unit and B accessible according to

$$g^3 = \left[\left(1 + \frac{B}{7}\right)^{0.5} + \frac{4B}{9\pi}\right]^{-0.5} \tag{11}$$

The branching density can further be estimated by the apparent density which is calculated from molar mass and R_{g} with

$$d_{\mathrm{APP}} = \frac{3}{4\pi N_A} \frac{M_w}{R_{\mathrm{g}}^3} \tag{12}$$

giving indications about the global compactness of the molecule in solution. When investigating the dilute solution state of polymers one has to determine the structural conformation which is possible by the radii ratios

$$\rho = \frac{R_{\mathrm{g}}}{R_{\mathrm{H}}} \tag{13}$$

and

$$\kappa = \frac{R_\eta}{R_{\mathrm{g}}}\ . \tag{14}$$

Mean-field models for branched polymers in good solvents

For describing the extension of a branched polymer R, we're using a Flory-type mean-field approach.[6] In the spirit of the Flory argument the excluded volume of N monomers in density field of the polymer is balanced by the total elastic contribution of all independent strands in the structure extended from their Gaussian conformation R_0. By further assuming a characteristic strand length of g monomers representing also the extension of the molecules without excluded volume $R_0^2 \sim b^2 \cdot g$ leads to a free energy approach in

good solvent[6]

$$F = u \cdot \frac{N}{g} \cdot \left(\frac{R^2}{R_0^2} \right) + \upsilon \cdot \frac{N^2}{R^3} \ , \tag{15}$$

where the prefactor u accounts for the a priori unknown elasticity constant and should be of order unity and can be adsorbed in the definition of energy and length scale, and υ denotes the strength of the excluded volume. Minimizing Eq. (15) with respect to R gives a relation for the equilibrium extension of the molecule[6]

$$R^2 = a^{2/5} \cdot N^{2/5} \cdot R_0^{8/5} \ , \tag{16}$$

where the factor $a = \left(\frac{3}{2}\frac{\upsilon}{u}\right)$ accumulates the constants in Eq. (15). A detailed discussion of this approach can be found in Ref.[6] The result allows a prediction of scaling of the extension of arbitrarily branched molecules based on the reference strand in the ideal case. As illustrative example, the extension of an ideal chain $R_0^2 \sim N$ leads to the known[7,8] excluded volume extension of a real linear chain $R_{\mathrm{L}}^2 \sim N^{6/5}$ with the Flory exponent $\nu = \frac{3}{5}$ close to the value of $\nu \simeq 0.588$ for linear chains[8]. A perfect dendrimer is characterized by the generation G and spacer length S between the branching points exhibiting an exponential growth $N \sim S \cdot e^G$. The characteristic length scale is given by $g = G \cdot S$ resulting in the logarithmic extension under ideal (not θ-solvent) conditions $R_0^2 \sim G \cdot S \sim S \ln(N)$, and according to Eq.(16) a mixed logarithmic-power-law behavior under excluded volume case

$$R_{\mathrm{DD}}^2 \sim N^{2/5} \cdot (GS)^{4/5} \sim N^{2/5} \cdot [S \ln(N/S)]^{4/5} \ . \tag{17}$$

The latter relation has been extensively proven in computer simulations.[6,9,10]

For a particular type of hyperbranched polymers obtained in a cluster-cluster aggregation mechanism already Zimm and Stockmayer[11] have predicted the result $R_0^2 \sim N^{1/2}$. Using Eq. (16) in previous work[6] the relation

$$R_{\mathrm{ZS}}^2 \sim N^{4/5} \tag{18}$$

has been derived and also supported by simulations[6,12] and in agreement with hyperscaling theory.[13]

Furthermore, the intrinsic viscosity $[\eta]$ can be related to the extension R and degree of polymerization N by the Flory-Fox equation[4,5] and therefore the Kuhn-Mark-Houwink-Sakurada equation with

$$[\eta] \sim \Phi \frac{R^3}{N} \sim K_\eta \cdot N^\alpha \tag{19}$$

with the Flory parameter Φ, the Mark-Houwink parameter K_η, and the exponent α related to the fractal dimension of the molecule if applicable. Hence, the mean field theory predict the relation for excluded volume structures as linear chains $[\eta_\mathrm{L}] \sim N^{4/5}$ and randomly hyperbranched $[\eta_\mathrm{ZS}] \sim N^{1/5}$, and bell shaped curve for dendrimers[14] $[\eta_\mathrm{DD}] \sim N^{-2/5} \cdot [S \ln\left(\frac{N}{S}\right)]^{6/5}$.

More local information on the structures can be provided by scattering experiments, where the scattering intensity $I(q)$ is related to the static structure factor. By definition the static structure factor $S(\vec{q})$ obeys the limiting cases for low $\vec{q}$ values $S(\vec{q} \to 0) = N$ and high $\vec{q}$ values $S(\vec{q} \to \infty) = 1$ and provides information about the internal structure by using Porod's law for large wave numbers[15]

$$I(q) \simeq S(q) \sim q^{-\chi} \sim q^{-1/\nu} \ , \tag{20}$$

where $q = |\vec{q}|$ is the magnitude of the scattering wave vector $\vec{q}$, χ is the Porod's scaling exponent (fractal dimension) related to the Flory exponent $\nu = \frac{1}{\chi}$ of the macromolecule. As the fractal dimension can be related to the size scaling of the molecule $R \sim N^{1/\chi}$ one expects $\chi_\mathrm{L} \simeq 5/3$ for linear chains and $\chi_\mathrm{ZS} \simeq 5/2$ for randomly hyperbranched polymer both under athermal solvent condition. Note, that the scaling exponents in Porod's law can only be observed if the self-similarity of the object holds also for substructures, which is not applicable for dendrimers and is not quit obvious for randomly hyperbranched structures, also. For convenience we introduce the form factor by normalizing the scattering function $P(q \cdot R) = \frac{1}{N} S(q \cdot R) = I(q)/I_0$ obtaining a scaling function for comparison of different degree of polymerization.

Using these concepts we have shown that hyperbranched polymers which are obtained by a slow random addition of monomers do not display the randomly hyperbranched behavior but can be understood as disordered dendrimers where Eq. (17) instead of Eq. (18) is obeyed.[6] The Table S1 summarizes the limiting cases of different polymer topologies.

Table S1: Expected power laws for different polymer topology in the ideal extension R_0, extension with excluded volume R_g, the intrinsic viscosity $[\eta]$, and Porod's scaling exponent χ.

topology	R_0^2	R_g^2	$[\eta]$	χ
linear	N	$N^{6/5}$	$N^{4/5}$	$\frac{5}{3}$
randomly hb	$N^{1/2}$	$N^{4/5}$	$N^{1/5}$	$\frac{5}{2}$
dendrimer	$S \ln N$	$N^{2/5} \cdot [S \ln \left(\frac{N}{S}\right)]^{4/5}$	$N^{-2/5} \cdot [S \ln \left(\frac{N}{S}\right)]^{6/5}$	not applicable

Dendritic blob model for chain walking topologies

As discussed in the main text for the case of walking catalysis, the two limiting cases of linear and dendritic growth have two merge for intermediate values of the walking rate w. At a characteristic length scale $\xi(w)$ the walker cannot explore the entire structure anymore. As consequence, the emerging structure can be considered as chain of "dendritic blobs". This length scale is related with a typical thread-length of a dendritic blob, which we call GS, and which corresponds to the average diffusive path the walker takes between two reaction events:

$$\tau \sim (GS)^2 \sim w \ . \tag{21}$$

Here, the typical time scale between two successive reaction events scales as $\tau \sim w$. There is an exponential relation between the number of monomers, $n_g \sim S\mathrm{e}^G$, in such a dendritic blob and the length of the thread, i.e. $n_g \sim \exp\left\{(\beta w)^{1/2}\right\}$, where we have introduced a numerical prefactor β. If the degree of polymerization is much smaller then n_g, the dendritic topology dominates. This behavior can be clearly seen in Fig. S13 for high w, where the radius of gyration follows the dendritic behavior.

As the degree of polymerization reaches n_g, the chain walker cannot cross the full structure within $w-1$ steps. As result a topology is created which is no more bound to

the existing structure. If we would follow the time in units of τ, each step now corresponds a possible reaction event (which adds a whole dendritic blob to the existing structure) and thus a linear structure emerges for times $t \gg \tau$. In this case the extension of the structure is that of an linear chain in good solvent which is composed of dendritic blobs of size ξ instead simple monomers:

$$R^2 \sim \xi^2 \left(\frac{N}{n_\mathrm{g}}\right)^{2\nu} \sim N^{2\nu} \exp\left[-\frac{4}{5}\left(\beta w\right)^{1/2}\right] \cdot \left(\beta w\right)^{2/5} \quad . \tag{22}$$

Thus, the branching density can be expressed using the contraction factor to its linear analogue $R_\mathrm{L}^2 \sim N^{2\nu}$ at equal molar mass N given by

$$g = \left(\frac{R^2}{R_\mathrm{L}^2}\right) \simeq \exp\left[-\frac{4}{5}\left(\beta w\right)^{1/2}\right] \cdot \left(\beta w\right)^{2/5} \quad . \tag{23}$$

The obtained structure for moderate values of w corresponds then to disordered dendritic bottle-brushes. However, since the degree of polymerization of the dendritic structure grows exponentially with w, see Eq. (21), the crossover towards a linear object can be shifted to extremely high molar masses for high values of w. This is the reason why we do not observe linear structures for $w > 10$ in our simulations, see Fig. S13. On the other hand, very dense dendritic bottle-brushes can be obtained for high values of w if the reaction goes on for long enough time to produce high molecular weight molecules.

Scattering Intensity

Results presented in this study are mainly obtained by static light scattering (SLS) and small angle neutron scattering (SANS). For both techniques, scattering is an outcome of the interaction between an incident beam (electromagnetic wave or particles) and a probing matter, resulting in an elastically emitted secondary beam. The interference of scattered radiation leads to amplification or extinction of the intensity and shows an angular dependence directly related to the structure of the sample. The scattering

intensity at a given angle θ is expressend by the excess Rayleigh ratio

$$R_\theta = \frac{I(q)}{I_0} r^2 \ , \tag{24}$$

where r is the distance between the scattering object and the detector, $I(q)$ is the scattering intensity at angle θ and I_0 is the intensity of the incident beam. The wavevector change q is related to the scattering angle and is given by

$$q = \left(\frac{4\pi n_0}{\lambda} \right) \sin \frac{\theta}{2} \tag{25}$$

It expresses the magnitude of the scattering vector and is often called the momentum transfer in SANS. λ is the wavelength of beam of light or neutrons and n_0 is the refractive index of solvent used in experiment, which in SANS is unity. The fundamental equation for scattered light of a macromolecule in dilute solution of concentration c is given by

$$\frac{K \cdot c}{R(\theta)} = \frac{1}{P(\theta)} \left(\frac{1}{M_w} + 2A_2 c + 3A_3 c^2 + ... \right) \ , \tag{26}$$

where M_w is the weight-average molar mass and A_2, $A_{3,...}$are virial coefficients which define the interactions between the macromolecule and solvent. The particle form factor $P(q)$ gives the angular dependence of the scattered light and K is the contrast factor which differs in SLS and SANS. In light scattering K is expressed by

$$K_{SLS} = \frac{4\pi^2}{\lambda^4 N_A} \left(n_0 \frac{\delta n}{\delta c} \right)^2 \ , \tag{27}$$

where $^{\delta n}/_{\delta c}$ is the refractive index increment and N_A is Avogadro´s number. In SANS the contrast is calculated by the difference in scattering length densities and is given by

$$K_{SANS} = \frac{(\rho_{b_1} - \rho_{b_0})^2}{c^2} \frac{\bar{v}_1}{N_A} \tag{28}$$

with

$$\rho_b = \frac{\sum \rho_i b_i}{\sum (m_i 1.66 \times 10^{-24})} \ . \tag{29}$$

Experimental data

Molecular properties of CWPE at various conditions

Table S2: Molecular properties of CWPE.

	RT-SEC in THF at T=25°C[a]				HT-SEC-D4 in TCB at T=150°C[b]		SANS in d-THF at T=25°C[c]			
Sample	M_n [kg/mol]	M_w [kg/mol]	M_n/M_w	R_g [nm]	M_n [kg/mol]	M_z [kg/mol]	R_q^{SANS} [nm]	χ	ν	A_2 [mol·l/g^2]
CWPE1	133.4 ± 3.9	162.9 ± 1.2	1.22	17.8 ± 0.2	164.2 ± 6.7	177.9 ± 3.7	18.6	1.38	0.73	2.40E-5
CWPE2	43.1 ± 1.3	51.3 ± 0.8	1.19	10.6 ± 0.3	50.7 ± 0.7	57.6 ± 0.9	11.3	1.50	0.67	1.52E-5
CWPE3	16.5 ± 0.1	18.8 ± 0.1	1.14	9.5 ± 0.1	22.0 ± 0.7	25.0 ± 0.3	6.1	1.58	0.63	1.08E-5
CWPE4	245.7 ± 10.6	331.9 ± 3.7	1.35	29.1 ± 0.1	343.1 ± 9.8	410.5 ± 7.2	18.3	1.64	0.61	3.63E-5
CWPE5	48.9 ± 2.2	58.3 ± 1.1	1.17	8.9 ± 1.4	66.3 ± 1.9	71.2 ± 1.9	7.4	2.09	0.48	3.57E-6
CWPE6	95.3 ± 3.0	130.0 ± 1.4	1.37	11.3 ± 0.7	156.6 ± 2.3	174.7 ± 0.7	13.9	1.96	0.51	2.99E-6
CWPE7	214.8 ± 14.9	229.4 ± 4.6	1.39	18.5 ± 0.1	326.0 ± 3.2	414.8 ± 3.4	17.8	2.05	0.49	3.38E-6
CWPE8	116.9 ± 8.5	171.4 ± 2.5	1.47	14.1 ± 0.3	169.1 ± 2.0	297.0 ± 3.2	12.0	2.22	0.45	2.71E-6
CWPE9	111.4 ± 3.7	139.2 ± 1.5	1.25	9.9 ± 0.3	152.1 ± 1.6	159.7 ± 1.5	11.8	2.14	0.47	2.03E-6
CWPEx	173.7 ± 6.1	219.7 ± 2.9	1.26	15.9 ± 1.3	141.1 ± 5.5	165.7 ± 1.7	12.9	2.28	0.44	1.57E-6

[a,b]All values and averages determined from triple determination. [c]Determined by Zimm-approach.

Conformation and Topology of CWPE from Multidetector-SEC.

Note that systems that theoretically exceed the lower resolution limits of LS (PE4, PE9) were found to be significantly smaller using SANS data. However, for PE5 the difference of R_g is quite severe with 18.3 nm and 30.4 nm for SANS and LS, respectively. In addition, LS experiment in THF supports the higher R_g value, whereby the size discrepancy cannot be legitimated by the solution state. Furthermore, comparing PE5 to its dendritic counterpart at low pressure (PE6) suggests that the true R_g is significantly larger than 17.3 nm. For other analyte pairs, the size difference of CWPEs synthesized at different pressure varies between $3.9 - 6.8$ nm depending on the polymerization time. Moreover, the synthesis temperature of 10°C was found to be an optimum for the catalytic activity that results in comparatively high radii and molar mass. $R_\mathrm{g} \sim 30nm$ as determined by SEC-MALLS is therefore quite convincing. We believe that the underestimate of $R_\mathrm{g}(PE5)$ origins from an insufficient q range at the lower limit.

Theoretical linear models for calculation of contraction factors:

$$[\eta_\mathrm{L}] = 5.3 \cdot 10^{-4} M_w^{0.7} \tag{30}$$

$$R_\mathrm{L} = 2.3 \cdot 10^{-2} M_w^{0.58} \tag{31}$$

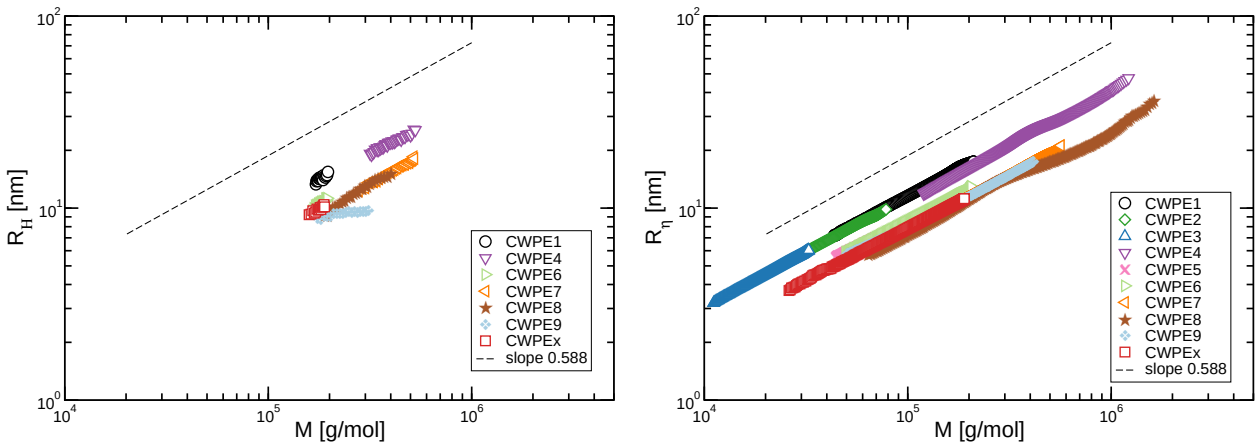

Figure S2: Conformation plots of CWPE obtained from HT-SEC-D4.

Table S3: Scaling exponents of CWPEs from conformation and KMHS plots determined by HT-SEC in 1,2,4-TCB. Two values stand for different molar mass regimes.

Sample	α	$\nu\,[R_g]$	$\nu\,[R_H]$	$\nu\,[R_\eta]$	g_w	g'_w	ε	λ
CWPE1	0.7	0.52	0.67	0.57	0.42 ± 6E-3	0.45 ± 9E-4	0.91 ± 2E-2	3.36 ± 0.09
CWPE2	0.71	0.78	-	0.57	0.48 ± 7E-3	0.42 ± 9E-4	1.18 ± 2E-2	12.77 ± 0.10
CWPE3	0.73	-	-	0.58	-	0.41 ± 1E-3	3.70 ± 1.20	30.80 ± 0.23
CWPE4	0.72/0.46	0.31/0.67	0.53	0.57	0.44 ± 5E-3	0.40 ± 5E-3	1.09 ± 2E-2	2.02 ± 0.03
CWPE5	0.49	-	-	0.51	0.26 ± 4E-2	0.21 ± 1E-2	1.19 ± 2E-1	64.25 ± 2.46
CWPE6	0.62	0.41	0.61	0.54	0.20 ± 6E-3	0.17 ± 5E-4	1.11 ± 2E-2	33.58 ± 0.23
CWPE7	0.66	0.45	0.59	0.56	0.17 ± 4E-3	0.14 ± 5E-4	1.12 ± 2E-2	22.65 ± 0.10
CWPE8	0.86/0.25	0.64/0.42	0.74/0.41	0.60/0.42	0.15 ± 8E-4	0.12 ± 5E-4	1.10 ± 3E-3	50.91 ± 0.79
CWPE9	0.6	0.31	0.16	0.52	0.16 ± 2E-3	0.13 ± 8E-4	1.13 ± 6E-3	67.71 ± 0.82
CWPEx	0.61	0.58	0.63	0.54	0.17 ± 3E-3	0.14 ± 4E-4	1.14 ± 1E-2	59.64 ± 1.08

Total number of branching per 1000 C atoms was calculated using

$$N_{Br} = \frac{2(I_{CH_3})}{3(I_{CH_3} + I_{CH_2} + I_{CH})} \times 1000 \tag{32}$$

by integrating methyl proton signals with respect to signals of all protons in the ^1H-NMR spectrum.

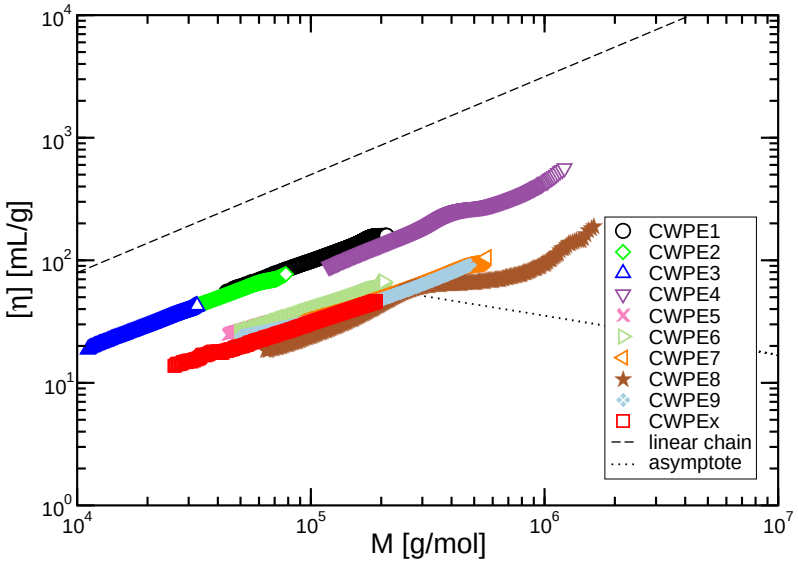

Figure S3: Kuhn-Mark-Houwink plot of CWPE obtained from HT-SEC-D4.

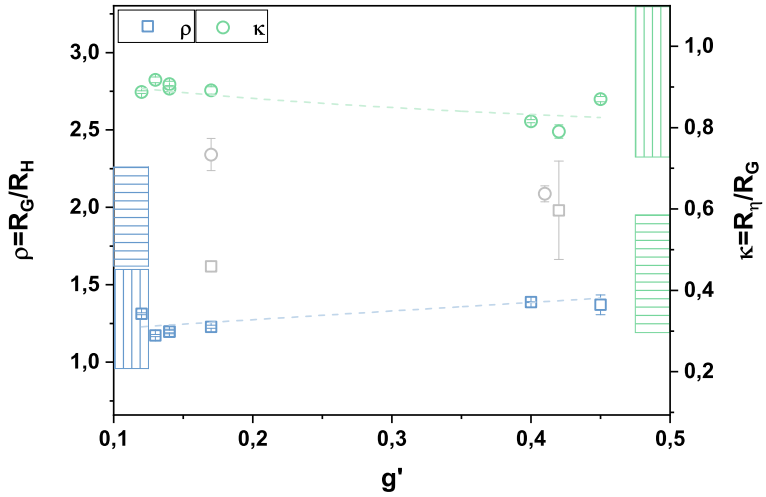

Figure S4: Structure factors ρ and κ as a function of g'. The cross-striped area marks range for linear coils, the along-striped area marks range for branched molecules.

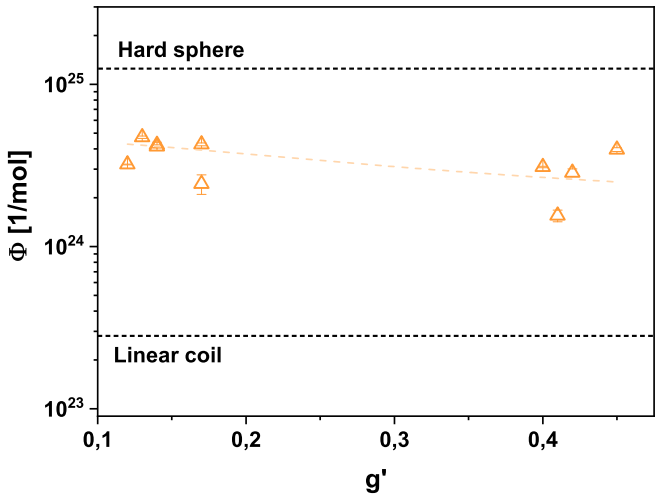

Figure S5: Flory-Fox parameter Φ as a function of g' of CWPEs obtained by HT-SEC-D4.

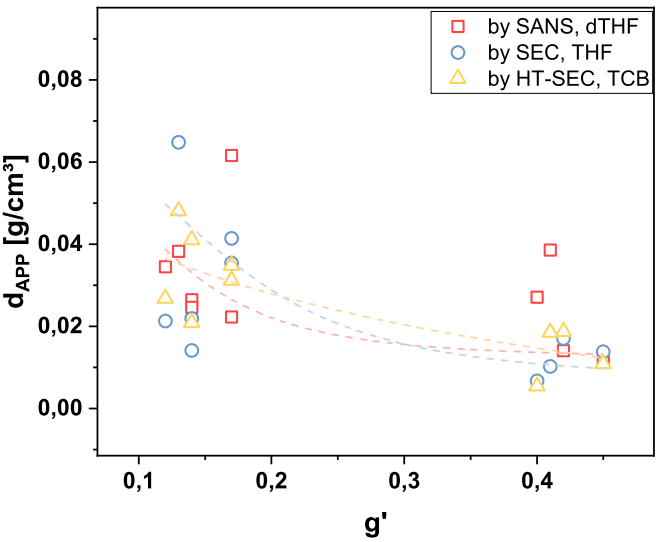

Figure S6: Apparent density vs. g' of CWPE obtained by HT-SEC-D4.

Table S4: Branching analysis from ^{1}H and ^{13}C NMR spectroscopy of CWPE.

	N_{Br}^{H}	N_{Br}^{C}	C1	C2	C3	C4	C5	C6+	ΣC4-C6+	sec-C4 [%]
CWPE1	98.1	100.1	34.1	16.4	4.5	9.1	3.2	22.0	36.5	9.7
CWPE2	114.3	104.7	34.9	16.3	4.1	6.7	3.2	25.6	35.5	9.5
CWPE3	107.0	110.1	35.3	16.7	3.8	7.0	3.1	26.0	43.8	11.1
CWPE4	101.0	90.4	33.5	15.2	2.8	7.1	2.6	24.3	33.9	10.0
CWPE5	126.5	110.1	28.5	17.4	1.7	7.5	1.6	31.5	40.6	14.5
CWPE6	100.9	85.0	27.2	16.2	14.7	3.7	1.0	30.9	35.5	12.6
CWPE7	104.9	111.0	28.2	18.0	1.7	7.4	1.6	32.0	41.0	15.5
CWPE8	100.6	93.7	29.4	15.8	13.0	3.4	1.7	30.1	35.2	15.4
CWPE9	98.9	108.6	27.9	17.9	1.7	7.6	1.5	32.1	41.2	13.7
CWPEx	105.6	122.0	26.4	16.7	10.0	3.0	1.5	28.7	33.2	13.8

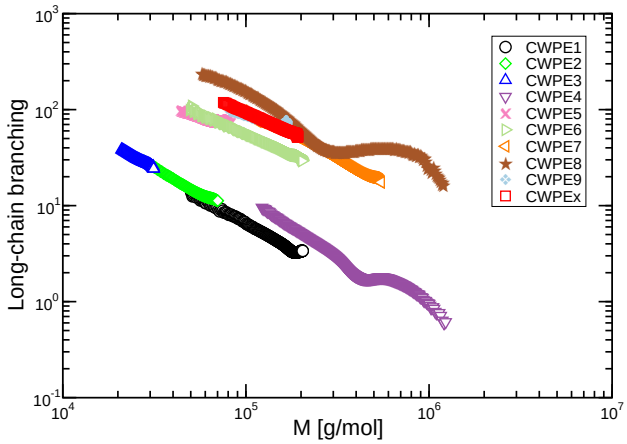

Figure S7: Long-chain branching as a function of molar mass of CWPE obtained by HT-SEC-D4.

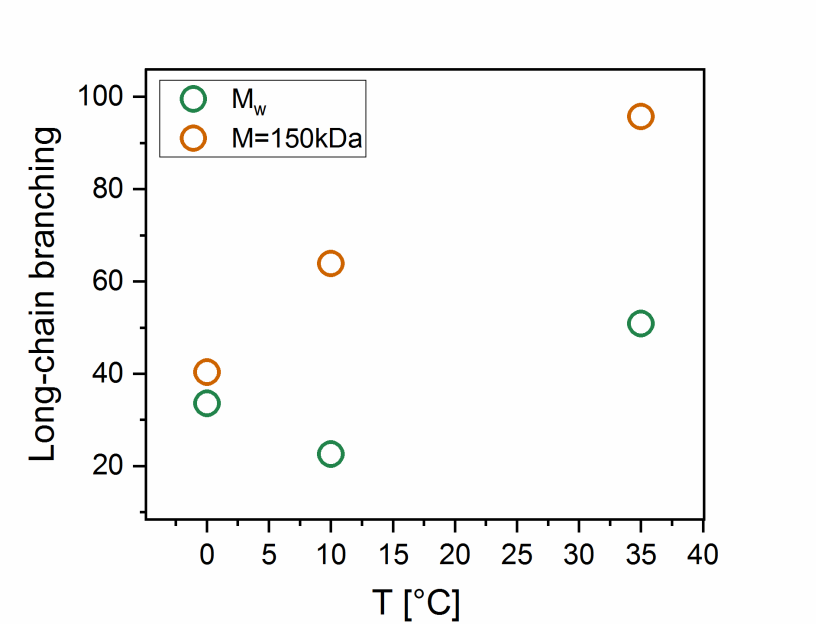

Figure S8: Synthesis-temperature dependence of long-chain branches in CWPE obtained from HT-SEC-D4.

Results from SANS Measurements

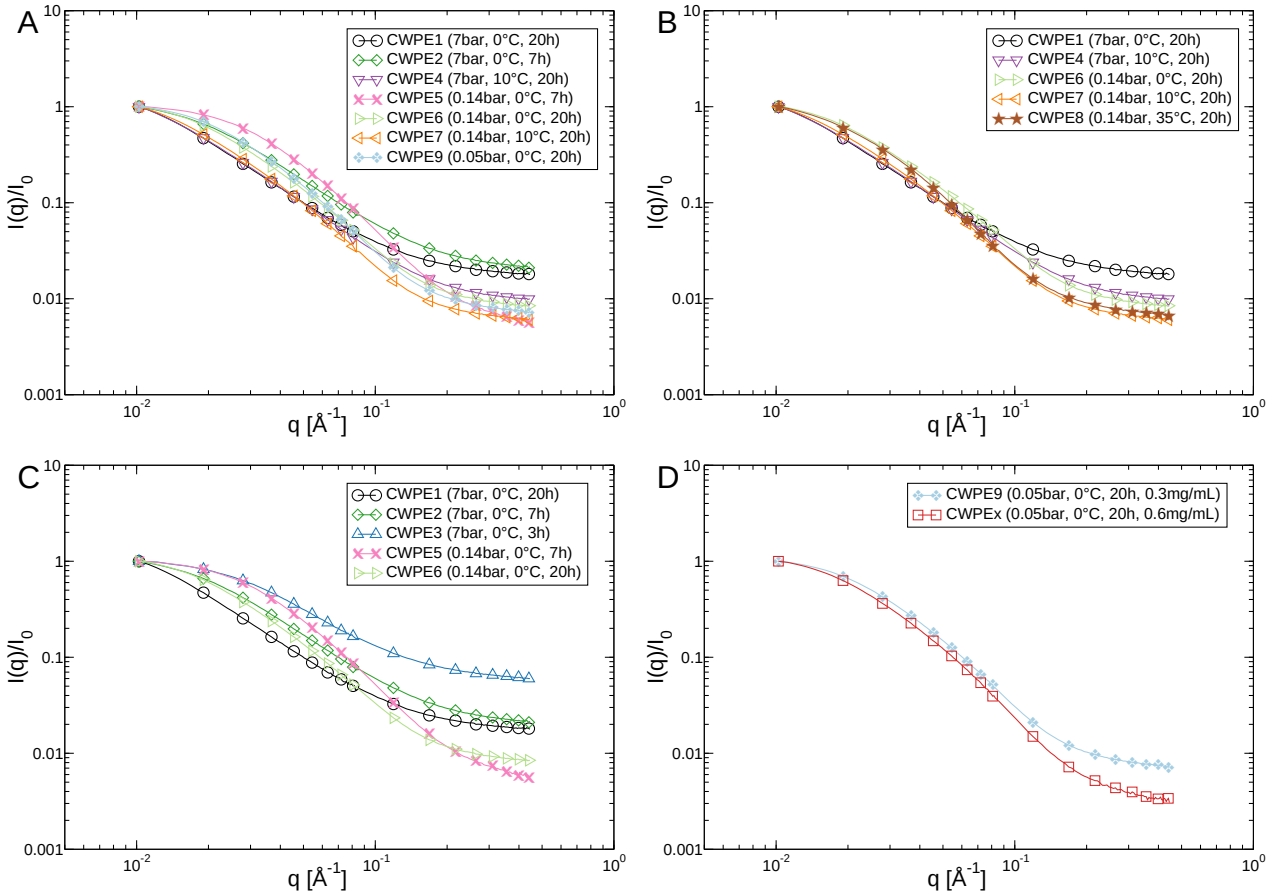

Figure S9: Normalized scattering intensity $I(q)/I_0$ vs. momentum transfer q of CWPE samples synthesized with varying pressure (A), temperature (B), time (C), and catalyst concentration (D). Most symbols are omitted for clarity.

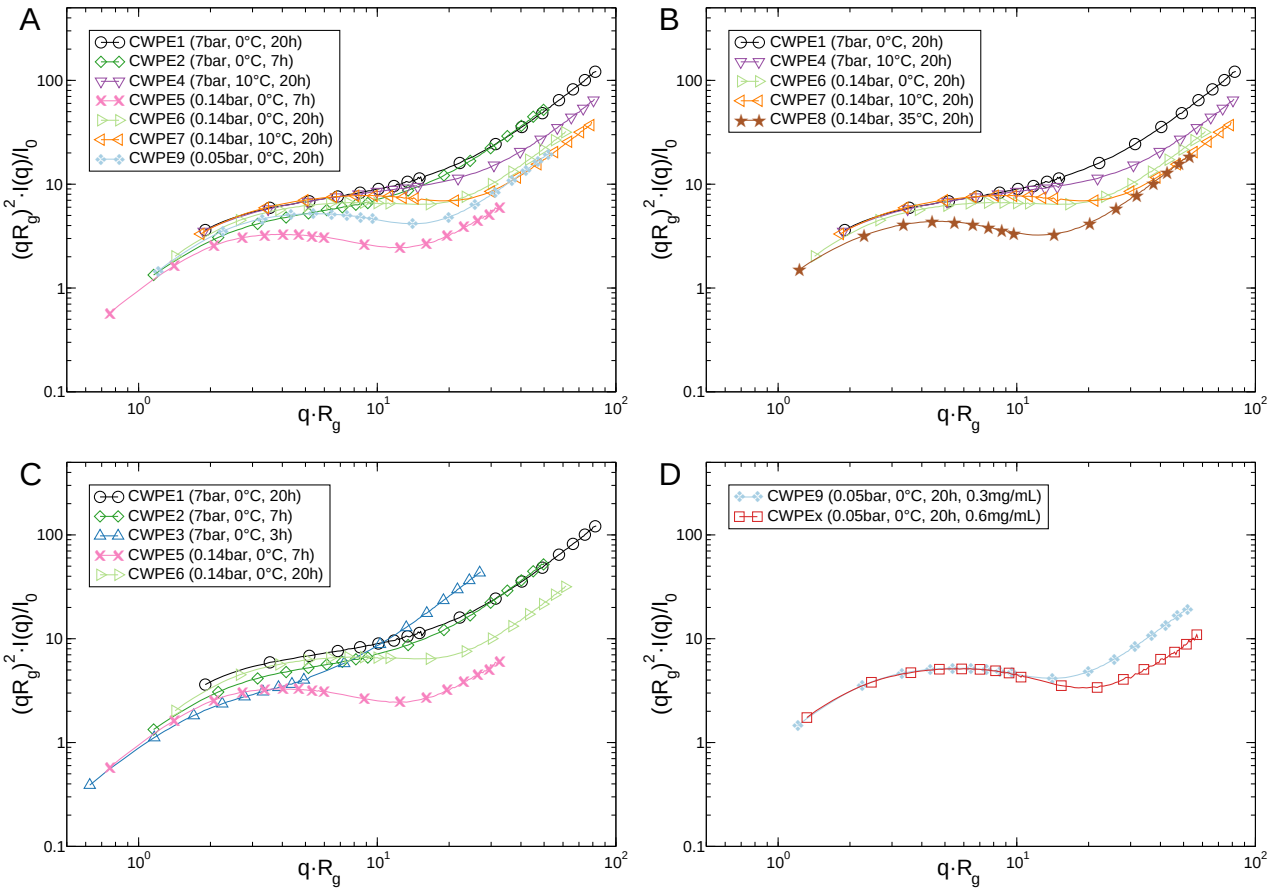

Figure S10: Kratky presentation of CWPE obtained from different reaction pressure at (A), temperature (B), time (C), and catalyst concentration (D).

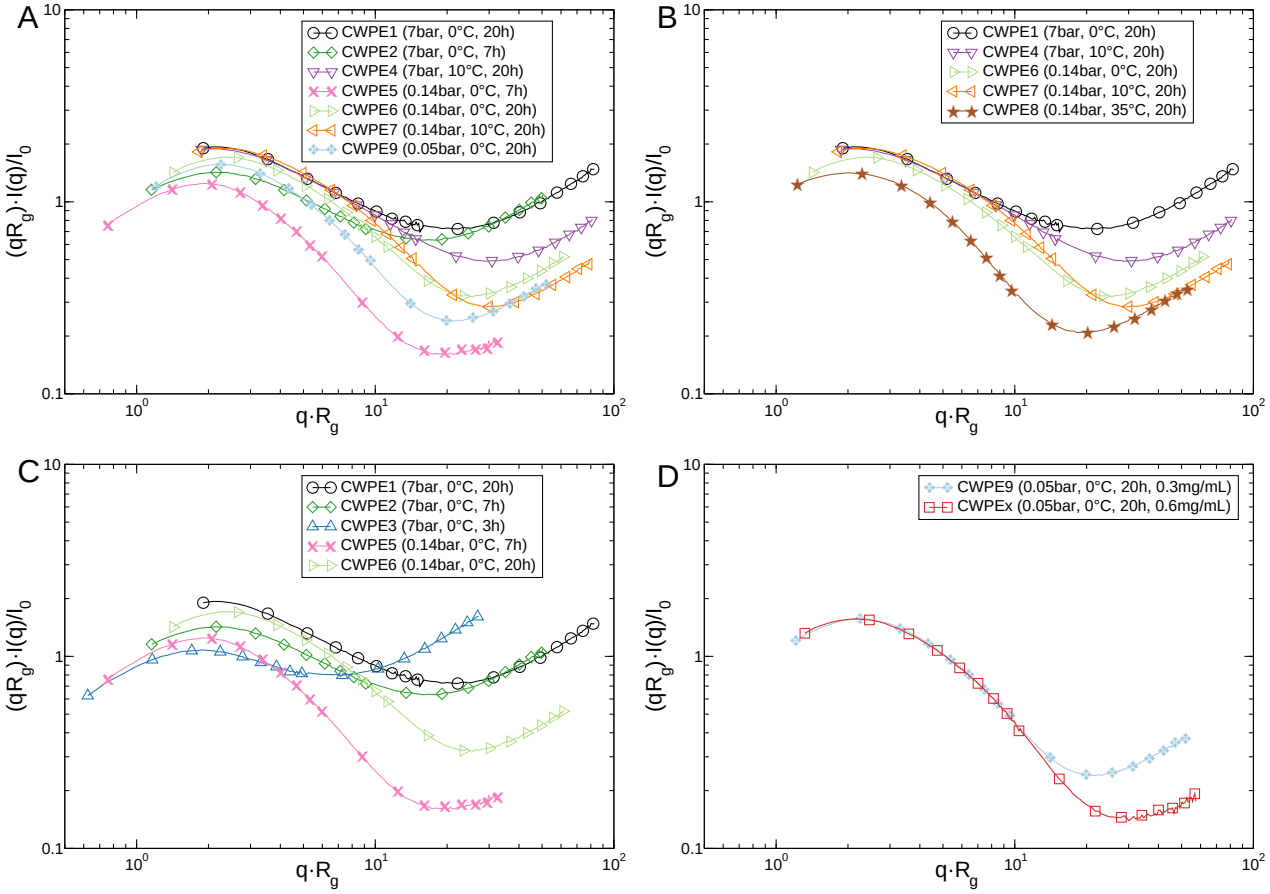

Figure S11: Casassa-Holtzer presentation of CWPE obtained from different reaction pressure at (A), temperature (B), time (C), and catalyst concentration (D).

Simulation Results

Simulation Method

We use the Bond Fluctuation Model[16,17] (BFM) to model the the chain walking catalyst mechanism under different walking/reaction probabilities p and to simulate the resulting flexible polymeric structures in good solvent conditions. In this coarse-grained Monte Carlo method polymers are modeled as connected cubes on a simple cubic lattice. One Monte Carlo sweep is implemented by moving a randomly chosen monomer in a randomly chosen move direction along the principal lattice axis. The bond vector set and the excluded volume condition are defined in a way to preserve the local and global topology and assure cut-avoidance. The move for a monomer is accepted if the new lattice positions are empty and all bond vectors connecting the structures are in the allowed set, otherwise the move is rejected. For the present case a set of 108 bonds with length $2, \sqrt{5}, \sqrt{6}, 3,$ and $\sqrt{10}$ is allowed and throughout this paper we set the length of one lattice site to unity. One Monte Carlo step (MCS) is defined as one attempted Monte Carlo move per monomer in average (sweep over all monomers) to be the time unit.

First, the CW structures with $N = 24; 32; \ldots; 2^k; \frac{3}{2}2^k; \ldots; 4096; 6144$ monomers for different chain walking rates w (reaction probabilities $p = 1/w$) are created in a cubic $L = 512$ simulation box as follows: we start with an initial configuration of $n = 2$ connected monomers. The metallocene catalysts is modeled as "walker" attribute on one particular monomer and placed randomly on the initial structure. The attachment and creation of a new monomer in the spirit of CW reaction is given as follows: First, the monomer with the walker attribute is tested if the functionality of the monomer is smaller than three rendering the chemical process only for trifunctional branching points. Second, as the CW structure is grown under excluded volume condition an additional test is necessary to ensure that the attachment and creation of a new monomer is possible within the BFM. Therefore, the vicinity of the walker monomer is tested for placement of a monomer in a shell of all permutations and sign combinations of the vector $P_{\pm}$ (2, 0, 0). The latter restriction ensures structures non-violating the global topology and enforces

the relaxation of the local structure. If one of the above criteria is not satisfied, the walker randomly moves to next connected neighbor and the structure is moved according to the BFM for 1000 monomer sweeps to relax the polymer and avoid regions with high density. Then the algorithm repeats to add a monomer as the structure still not contains the desired number of monomers $n \neq N$. Checking the functionality and the vicinity of the monomer is not sufficient for adding a monomer into the structure. To take into account the reaction/walking probability p, an additional acceptance-rejection conditions[18] has to be applied by dicing a uniformly distributed random number $\xi \in [0; 1)$ and compare to the reaction/walking probability $p \in [0; 1]$. If $\xi < p$ a new monomer is added to the walker monomer and the counter n is increased, otherwise the trial addition is rejected and the walker is moving on the structure with $1 - p$. After this step, the catalyst is placed either on the position of the added monomer (addition) or has moved to the next connected neighbors without preference of creational bias (walking). The structure is relaxed for 1000 MCS in both cases to equilibrate high density regions. If the number of monomers in the structure equals the desired number of monomers $n \equiv N$, the algorithm terminates, otherwise its repeats for adding a monomer. As stated above, for high p / low w the creation and attachment of monomer is most likely, whereas the walker movement is suppressed leading to linear structures (slow walking probability/high reaction probability) with the limiting case $w = p = 1$ as linear chain without branching. For low p / high w, the attachment of monomers is suppressed, whereas the walker moves along the structure forming highly branched polymeric structures (fast walking probability/low reaction probability). Note, that considering a trifunctional monomer as additional barrier for walking, does not effect the underlying topology, instead the transition region is shifted to higher molecular mass only. Within the algorithm the excluded volume condition is satisfied at all time steps leading to conformations suitable within the BFM. After the creation of the structures, one simulation run is performed to relax the branched polymer and equilibrate high density regions followed by a simulation run in order of magnitude 10^9 MCS for sampling the observables. As the algorithm produces only single highly branched structures (no detachment of the walker is considered), a set of at least 20 runs

are performed to provide an ensemble average for different N and $w = 1/p$. Throughout the paper, sampling the observables involves the ensemble average $\langle \dots \rangle_E$ of the time average $\langle \dots \rangle_t$ with the short-hand notation $\mathcal{A} \coloneqq \langle \mathcal{A} \rangle = \langle \langle \mathcal{A} \rangle_t \rangle_E$. For comparison of the obtained CW structures, additional simulations of linear chains, perfect tri-functional dendrimers, and Zimm-Stockmayer AB_2-distributed hyperbranched polymers[6] are performed. The perfect dendrimers are generated for different generation $G = 2$, ..., 10 with spacer length $S = 1$ and $S = 2$ between the branching units. To emphasize the difference between the CW structures and Zimm-Stockmayer hyperbranched polymers (rHB), a cluster-cluster aggregation mechanism is also used as we reported recently[6]. The BFM algorithm, simulations and evaluations of the data are performed by the C++ framework LeMonADE developed in our group[19].

Modeling the BFM to the Experiment

As the BFM operates on coarse-grained scales, the intrinsic length scale of one Kuhn length L_K within the BFM is used to match the experimental data. For PE[20] the bond length between -C-C- is given by $l_{PE} = 1.54\,\mathring{A}$ with a bond angle $\alpha = 112°$ providing a projected bond length $d_{PE} = l_{PE} \cdot \sin(\frac{\alpha}{2}) = 1.26\,\mathring{A}$. The contour length is given by $L = d_{PE} \cdot n$ with n as number of C-atoms along the backbone. To represent a equivalent freely jointed chain with extension $R = L_K \cdot N$ and $R^2 = C_\infty n l_{PE}^2 = N L_K^2 = L_K \cdot L$ with N Kuhn segments under a characteristic ratio $C_\infty = 7.2$ yields $L_K = \frac{C_\infty l_{PE}^2}{d_{PE}} = 13.4\,\mathring{A}$. For PE the number of repeating units of a molecule with molar mass M is given by $N = \frac{M}{M_0} \cdot \frac{b_{PE}}{L_K}$ taking into account the chemical monomeric segment length $b_{PE} = 2d_{PE}$ and $n = \frac{M}{M_0/2}$ for PE with molar mass of chemical unit $M_0 = 28\,\mathrm{g/mol}$. Thus, one BFM unit corresponds to 5.4 chemical PE monomers with 10.7 carbon atoms, see Tab. S5.

Table S5: Molar mass M_w of CWPEs determined by RT-SEC in THF and the corresponding Kuhn segments N in the BFM.

Sample	M_w [kg/mol]	N
CWPE1	162.9 ± 1.2	1094 ± 8
CWPE2	51.3 ± 0.8	345 ± 5
CWPE3	18.8 ± 0.1	126 ± 1
CWPE4	331.9 ± 3.7	2229 ± 25
CWPE5	58.3 ± 1.1	392 ± 6
CWPE6	130.0 ± 1.4	873 ± 9
CWPE7	229.4 ± 4.6	1541 ± 31
CWPE8	171.4 ± 2.5	1151 ± 17
CWPE9	139.2 ± 1.5	935 ± 10
CWPEx	219.7 ± 2.9	1476 ± 19

Radius of Gyration of Ideal Structures

The ideal radius of gyration, R^2_{g0}, is generally given by the connectivity matrix of any polymer structure according to the equation

$$R^2_{g0} = \frac{1}{N} \sum_{k=2}^{N} \frac{1}{\lambda_k} \, . \tag{33}$$

Here, λ_k denotes the k-th eigenvalue of the connectivity matrix (Rouse matrix) and the sum extents over all non-zero eigenvalues[21,22]. See Fig. S12.

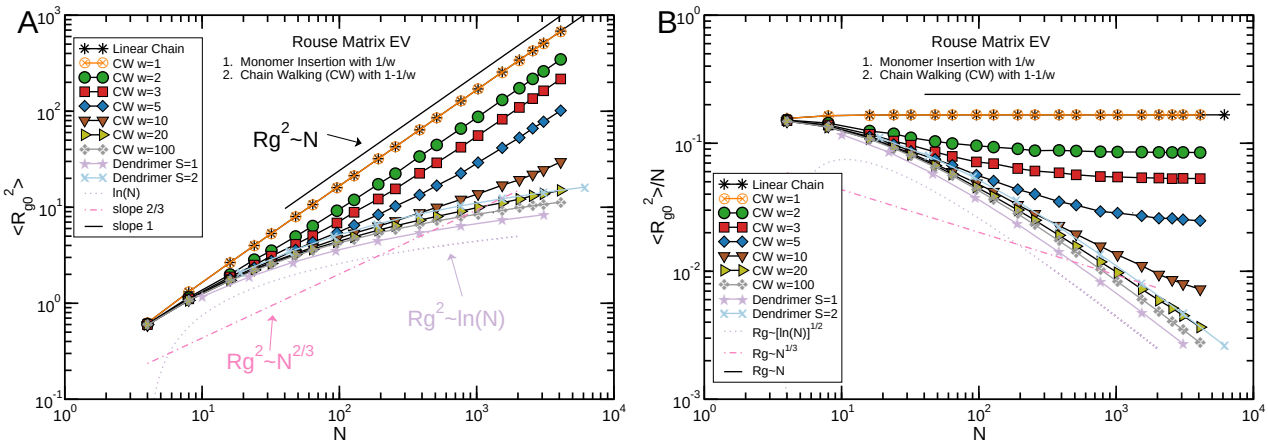

Figure S12: (A) Ideal radius of gyration R^2_{g0} CW-structures, dendrimer, and linear emphasizing the ideal chain behavior for high degrees of polymerization N. (B) Same data rescaled to ideal chain behavior $R^2_{g0} \sim N$.

Radius of Gyration and Intrinsic Viscosity of Excluded Volume Structures

The radius of gyration R_g^2 is calculated by

$$R_g^2 = \left\langle \frac{1}{N} \sum_{i=1}^{N} (\vec{r}_i - \vec{r}_{COM})^2 \right\rangle \ , \tag{34}$$

where the position of the i-th monomer is denoted by $\vec{r}_i$, $\langle \dots \rangle$ is the ensemble average of the time average and $\vec{r}_{COM} = \frac{1}{N} \sum_{j=1}^{N} \vec{r}_j$ is the center of mass. The average bond length inside the polymeric structure is defined as $b^2 = \langle (\vec{r}_i - \vec{r}_j)^2 \rangle_{\{i,j\}}$,where the ensemble-time average $\langle \dots \rangle_{\{i,j\}}$ is only calculated over all connected next neighbors. In Fig. S13 the data for the CW structures under excluded volume conditions rescaled by linear chain behavior ($R_g^2 \sim N^{2\nu}$) is depicted.

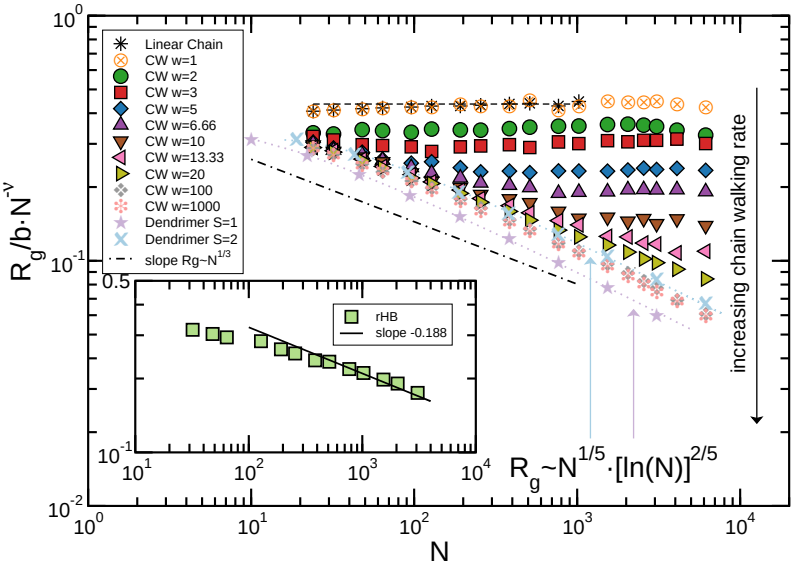

Figure S13: Radius of gyration R_g^2 of the CW structure scaled by linear chain behavior obtained for different walking rate w and various degree of polymerization N. The inset shows data for randomly hyperbranched (rHB) polymers.

Using the Flory-Fox equation $[\eta] \sim \Phi \frac{R^3}{N}$ with the mean-field result for R_g^2 yields the prediction for randomly hyperbranched $[\eta_{rHB}] \sim N^{1/5}$ and bell shaped curve for dendrimers $[\eta_{DD}] \sim N^{-2/5} \cdot [S \ln\left(\frac{N}{S}\right)]^{6/5}$. In Fig. S14 the predicted behavior for the CW-structures is depicted.

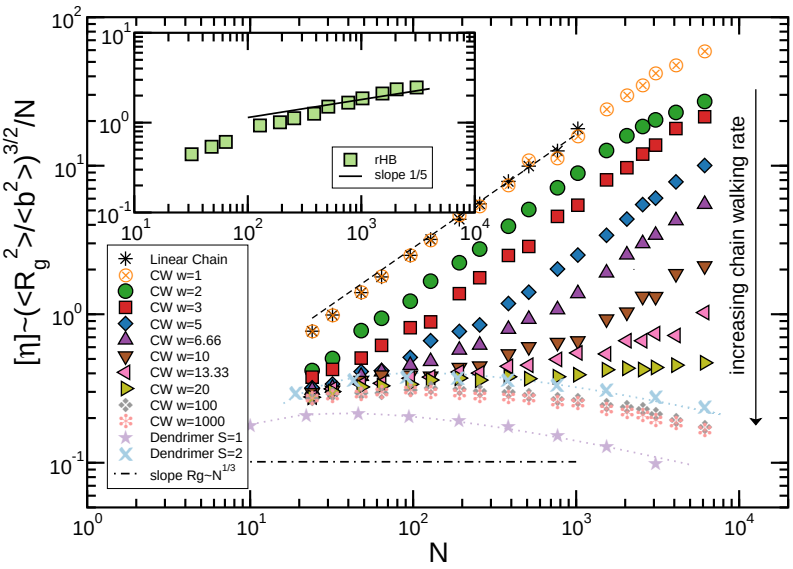

Figure S14: Predicted intrinsic viscosity $[\eta]$ by the Flory-Fox equation for the CW-structures with excluded volume.

Degree of Branching for CW-structures

As one particular topological measure the degree of branching DB of an AB_2 hyperbranched polymer is defined by[23,24]

$$DB = \frac{D+T}{D+T+L}\,, \tag{35}$$

where L, T, D denote the linear (two-functional), terminal (mono-functional), and dendritic (three-functional) groups of the molecules, respectively. For linear chains ($w = 1$) the degree of branching reads $DB \simeq 0$, randomly hyperbranched polymers $DB = 0.5$, and for dendrimers the degree of branching $DB = \frac{1}{S}$ is inverse proportional to spacer length S. Any plateau-like behavior is related to (linear or dendritic) bottle-brush behavior providing sufficient dendritic groups (see Fig. S15). Similarly to the experiment, the branching number N_{Br} for the simulation data is calculated by

$$N_{\mathrm{Br}} = \frac{T}{D+T+L} = \frac{T}{N} \tag{36}$$

and converted to experimental units using the previous described mapping.

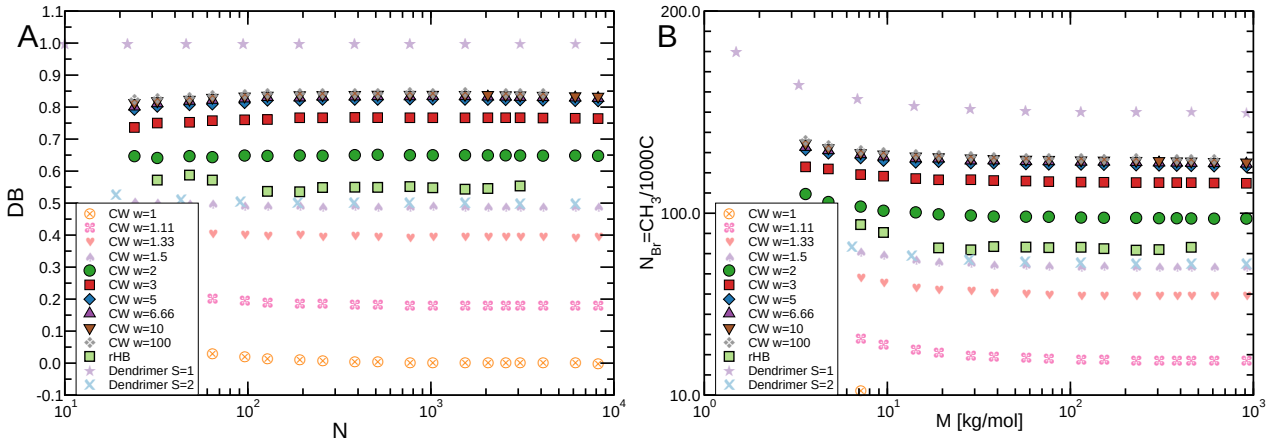

Figure S15: (A) Degree of Branching DB obtained for the CW structures as function of the degree of polymerization N and walking rate w for CW structures. (B) Same simulation data converted to branching number N_{Br} in experimental units.

Scattering Intensity

For the internal structure, the static scattering function $S(\vec{q})$ of the polymers defined as

$$S(\vec{q}) = \left\langle \frac{1}{N} \sum_{i,j=1} \exp\left[-i\vec{q}(\vec{r}_{\mathrm{i}} - \vec{r}_{\mathrm{j}})\right] \right\rangle \tag{37}$$

with the scattering wave vector $\vec{q}$ assuming N identical monomers at the position vector $\vec{r}_{\mathrm{i/j}}$. For low polymer concentrations, the scattering intensity is proportional to the static structure factor[25] $I(\vec{q}) \simeq S(\vec{q})$ as we neglect inter-particle interference in the computer simulations considering scattering only by one molecule. For convenience we introduce the form factor by normalizing the scattering function $P(q \cdot R) = \frac{1}{N} S(q \cdot R) = I(q)/I_0$ obtaining a scaling function for comparison of different degree of polymerization.

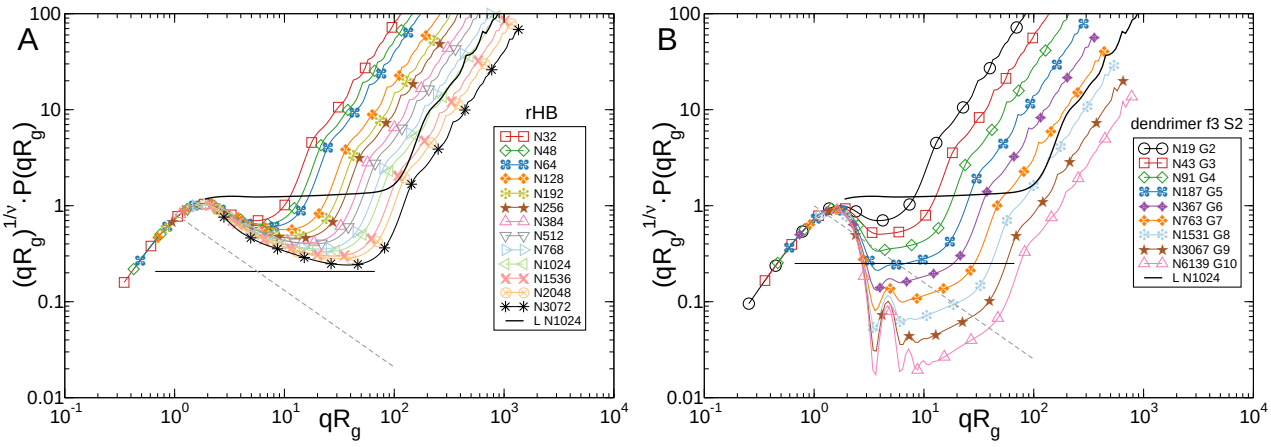

Figure S16: Scattering plot in the modified Kratky-representation for (A) randomly hyperbranched molecules and (B) perfect trifunctional dendrimers with $S = 2$. The black solid line indicates the expected slope for a linear chain $P(q \cdot R_g) \sim q^{-1/\nu}$ and simulation data for $N = 1024$, whereas the gray stroked line corresponds to the mean-field prediction $P(q) \sim q^{-5/2}$ for rHB. Most of the symbols are omitted for clarity.

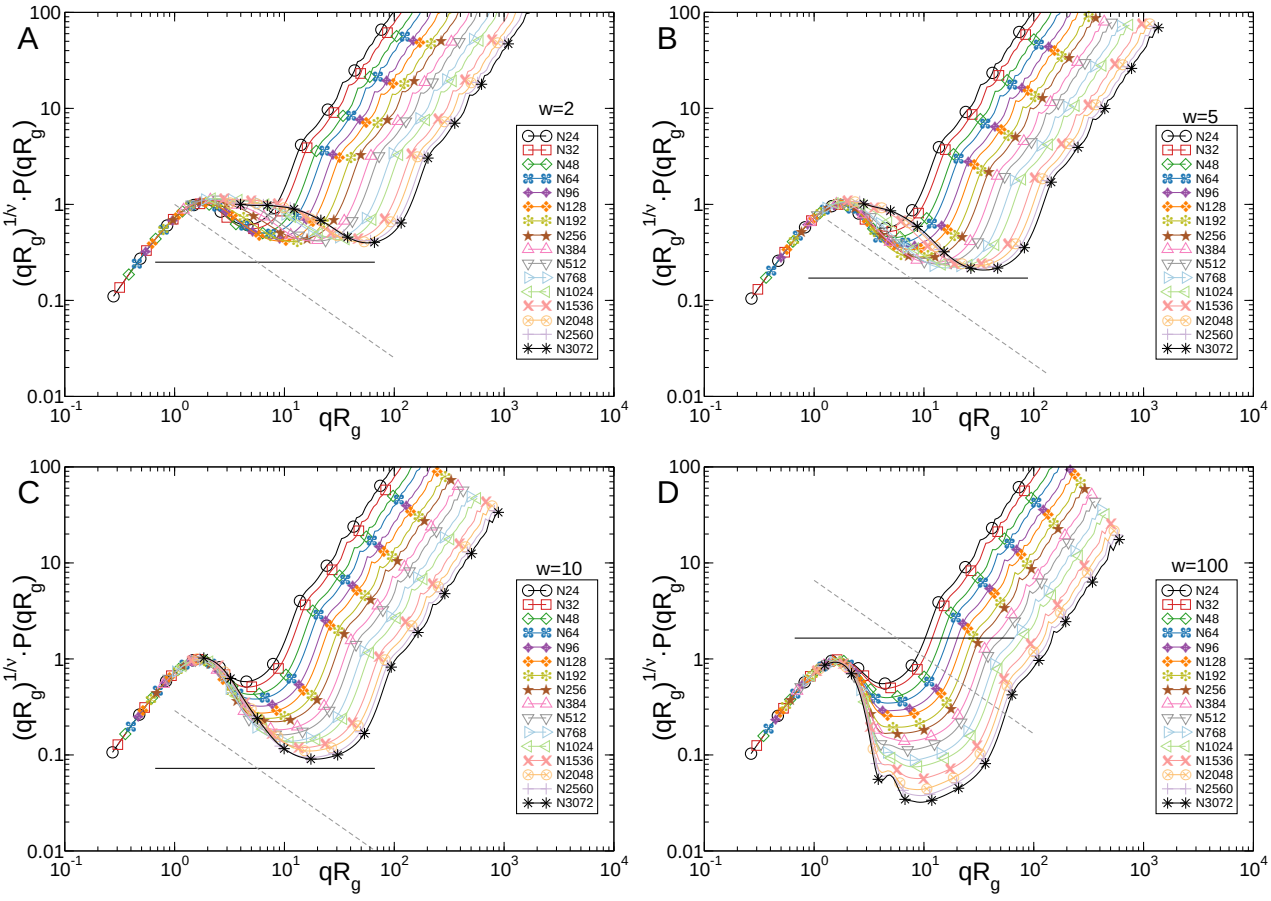

Figure S17: Scattering plot in the modified Kratky-representation for CW structures with walking rate $w = 2\,(\mathrm{A}), 5\,(\mathrm{B}), 10\,(\mathrm{C})$, and $w = 100\,(\mathrm{D})$ in comparison to randomly hyperbranched and linear chain scaling. The black solid line indicates the expected slope for a linear chain $P(q) \sim q^{-1/\nu}$, whereas the gray stroked line corresponds to the mean-field prediction $P(q) \sim q^{-5/2}$ for rHB. Most of the symbols are omitted for clarity.

References

(1) Galland, G. B.; de Souza, R. F.; Mauler, R. S.; Nunes, F. F. 13C NMR Determination of the Composition of Linear Low-Density Polyethylene Obtained with [η3-Methallyl-nickel-diimine]PF6 Complex. *Macromolecules* **1999**, *32*, 1620–1625.

(2) Johnson, L. K.; Killian, C. M.; Brookhart, M. New Pd(II)- and Ni(II)-Based Catalysts for Polymerization of Ethylene and α-Olefins. *J. Am. Chem. Soc.* **1995**, *117*, 6414–6415.

(3) Mecking, S.; Johnson, L. K.; Wang, L.; Brookhart, M. Mechanistic Studies of the Palladium-Catalyzed Copolymerization of Ethylene and α-Olefins with Methyl Acrylate. *J. Am. Chem. Soc.* **1998**, *120*, 888–899.

(4) Fox, T. G.; Flory, P. J. Second-Order Transition Temperatures and Related Properties of Polystyrene. I. Influence of Molecular Weight. *J. Appl. Phys.* **1950**, *21*, 581–591.

(5) Fox, T. G.; Flory, P. J. The glass temperature and related properties of polystyrene. Influence of molecular weight. *J. Polym. Sci.* **1954**, *14*, 315–319.

(6) Jurjiu, A.; Dockhorn, R.; Mironova, O.; Sommer, J.-U. Two universality classes for random hyperbranched polymers. *Soft Matter* **2014**, *10*, 4935–4946.

(7) Flory, P. J. *Principles of Polymer Chemistry*; Cornell University Press: Ithaca, New York: Ithaca, United States, 1953.

(8) De Gennes, P.-G. *Scaling Concepts in Polymer Physics*; Cornell University Press: Ithaca, New York, 1979.

(9) Kłos, J. S.; Sommer, J.-U. Properties of Dendrimers with Flexible Spacer-Chains: A Monte Carlo Study. *Macromolecules* **2009**, *42*, 4878–4886.

(10) Wengenmayr, M.; Dockhorn, R.; Sommer, J.-U. Multicore Unimolecular Structure Formation in Single Dendritic-Linear Copolymers under Selective Solvent Conditions. *Macromolecules* **2016**, *49*, 9215–9227.

(11) Zimm, B. H.; Stockmayer, W. H. The Dimensions of Chain Molecules Containing Branches and Rings. *J. Chem. Phys.* **1949**, *17*, 1301–1314.

(12) Wang, L.; He, X. Conformation of nonideal hyperbranched polymer in AB_n (n = 2, 4) type polymerization. *J. Polym. Sci., Part B: Polym. Phys.* **2010**, *48*, 610–616.

(13) Rubinstein, M.; Colby, R. H. *Polymer Physics*; Oxford University Press Inc.: New York, 2003.

(14) Giupponi, G.; Buzza, D. M. A. Monte Carlo simulation of dendrimers in variable solvent quality. *J. Chem. Phys.* **2004**, *120*, 10290–10298.

(15) Porod, G. Die Röntgenkleinwinkelstreuung von dichtgepackten kolloiden Systemen. *Kolloid-Zeitschrift* **1951**, *124*, 83–114.

(16) Carmesin, I.; Kremer, K. The bond fluctuation method: a new effective algorithm for the dynamics of polymers in all spatial dimensions. *Macromolecules* **1988**, *21*, 2819–2823.

(17) Deutsch, H. P.; Binder, K. Interdiffusion and self-diffusion in polymer mixtures: A Monte Carlo study. *J. Chem. Phys.* **1991**, *94*, 2294–2304.

(18) von Neumann, J. In *Monte Carlo Method*; Householder, A. S., Forsythe, G. E., Germond, H. H., Eds.; National Bureau of Standards Applied Mathematics Series; US Government Printing Office: Washington, DC, 1951; Vol. 12; Chapter 13, pp 36–38.

(19) Dockhorn, R.; Rabbel, H.; Werner, M.; Jentzsch, C.; Wengenmayr, M. LeMonADE-project. 2015; `https://github.com/LeMonADE-project/LeMonADE`.

(20) Vasile, C.; Pascu, M. *Practical Guide to Polyethylene*; 2005.

(21) Sommer, J.-U.; Schulz, M.; Trautenberg, H. L. Dynamical properties of randomly cross-linked polymer melts: A Monte Carlo study. I. Diffusion dynamics. *J. Chem. Phys.* **1993**, *98*, 7515–7520.

(22) Sommer, J.-U.; Blumen, A. On the statistics of generalized Gaussian structures: collapse and random external fields. *J. Phys. A: Math. Gen.* **1995**, *28*, 6669–6674.

(23) Hawker, C. J.; Lee, R.; Frechét, J. M. J. One-Step Synthesis of Hyperbranched Dendritic Polyesters. *J. Am. Chem. Soc.* **1991**, *113*, 4583–4588.

(24) Hölter, D.; Burgath, A.; Frey, H. Degree of branching in hyperbranched polymers. *Acta Polym.* **1997**, *48*, 30–35.

(25) Strobl, G. *The Physics of Polymers*, 3rd ed.; Springer-Verlag: Berlin, 2007.